

Realistic fault detection of li-ion battery via dynamical deep learning

Received: 18 May 2023

Accepted: 21 August 2023

Published online: 23 September 2023



Jingzhao Zhang^{1,2,10}, Yanan Wang^{3,10}, Benben Jiang^{4,10}, Haowei He¹, Shaobo Huang⁵, Chen Wang⁶, Yang Zhang⁵, Xuebing Han³, Dongxu Guo³, Guannan He^{7,8,9}✉ & Minggao Ouyang³✉

Accurate evaluation of Li-ion battery (LiB) safety conditions can reduce unexpected cell failures, facilitate battery deployment, and promote low-carbon economies. Despite the recent progress in artificial intelligence, anomaly detection methods are not customized for or validated in realistic battery settings due to the complex failure mechanisms and the lack of real-world testing frameworks with large-scale datasets. Here, we develop a realistic deep-learning framework for electric vehicle (EV) LiB anomaly detection. It features a dynamical autoencoder tailored for dynamical systems and configured by social and financial factors. We test our detection algorithm on released datasets comprising over 690,000 LiB charging snippets from 347 EVs. Our model overcomes the limitations of state-of-the-art fault detection models, including deep learning ones. Moreover, it reduces the expected direct EV battery fault and inspection costs. Our work highlights the potential of deep learning in improving LiB safety and the significance of social and financial information in designing deep learning models.

Achieving net-zero emissions entails transportation electrification^{1,2} and decarbonization³. Electric vehicles (EVs) with lithium-ion batteries (LiBs) are the most widely adopted devices due to their rapid performance improvements and cost reductions^{4–6}. One major concern to EV owners and manufacturers is battery safety^{7,8}. EV fires last longer and are more unpredictable, requiring frequent costly inspections for EV manufacturers. Therefore, early prediction of battery failure events could save significant social costs and promote EV adoption. However, as EV batteries are highly complex nonlinear systems, designing algorithms that understand the failure mechanisms—including short circuit, physical damage, overcharge/overdischarge, thermal abuse, etc.^{9–12}—remains challenging.

Existing studies on battery safety have explored both physics-based^{13–17} and data-driven^{18–25} approaches to address issues caused by defective battery cells. However, applying these methods in real life still has a long way to go for two reasons. First, existing algorithms require further testing, as validations are only done in small-scale experimental/lab settings. In contrast, the success of data science in many other fields, such as video games, vision, translation and protein structure predictions, were developed and evaluated on large-scale, real-world datasets^{26–29}. Second, many existing algorithms rely on information that is unavailable in real-world settings. Designing an EV battery fault detection algorithm that is implementable and effective for both EV manufacturers and owners needs to take practical social

¹IIS Tsinghua University, Beijing, China. ²Shanghai Qizhi Institute, Shanghai, China. ³State Key Laboratory of Intelligent Green Vehicle and Mobility, School of Vehicle and Mobility, Tsinghua University, Beijing, China. ⁴Department of Automation, Beijing National Research Center for Information Science and Technology, Tsinghua University, Beijing, China. ⁵Beijing Circue Energy Technology Co. Ltd., Beijing, China. ⁶School of Automation Science and Electrical Engineering, Beihang University, Beijing, China. ⁷Department of Industrial Engineering and Management, College of Engineering, Peking University, Beijing, China. ⁸National Engineering Laboratory for Big Data Analysis and Applications, Peking University, Beijing, China. ⁹Peking University Changsha Institute for Computing and Digital Economy, Changsha, China. ¹⁰These authors contributed equally: Jingzhao Zhang, Yanan Wang, Benben Jiang.

✉ e-mail: gnhe@pku.edu.cn; ouymg@tsinghua.edu.cn

factors into account^{30,31}, such as the data availability, economic trade-offs, sensor noise, and model privacy. In short, existing studies do not reveal the power of deep learning for EV battery fault detection with large-scale publicly available EV charging datasets, nor do they discover how practical factors should inform algorithm design and deployment.

In this work, we release three EV charging datasets with over 690,000 charging snippets from 347 EVs. Our datasets enable us to benchmark known deep learning models and compare them against the more conventional data-driven approaches. We found that although all models can achieve nontrivial detection power (as measured by accuracy and recall) by learning from the data, their performances could incur high economic costs, which are around 10³ Chinese Yuan (CNY) per vehicle according to our computation.

To address the problem, we further develop a deep learning model termed dynamical autoencoder for anomaly detection (DyAD) with a privacy-friendly and communication-efficient design. Our proposed model is the first deep learning model tailored for large-scale real-world EV LiBs data. It exploits the hidden Markov model of battery data in designing the neural network training pipeline and balances EV LiB accident costs against inspection costs based on empirical statistics. Our model differs from existing deep anomaly detection models in two aspects. First, it adopts a dynamical system formulation and partitions the data features into system inputs and system responses. It then detects the abnormality in the input-to-response mappings. In contrast, most existing deep learning algorithms for fault detection treat each dimension of the data features equally and is not tailored for dynamical system with external inputs. Second, our model exploits the

structure in EV fault labels by bridging the predictions between the vehicle system level and the LiB charging snippet level with a robust scoring procedure. We test our proposed algorithm on the three datasets with 55 abnormal vehicles (vehicles with LiB fault) and 292 normal vehicles (vehicles without LiB fault). Compared with conventional physics-based methods and the state-of-the-art deep learning models, our algorithm produces a dominating average receiver operating characteristic (ROC) curve for predicting LiB anomalies, and it lowers the overall costs (33–50% savings) of EV battery accidents and inspections. This work highlights the effectiveness of deep-learning algorithms in predicting EV LiB faults with limited anomaly samples and the practicality of our algorithm design.

Results

Challenges in real-world EV battery fault detection

Real-world anomaly detection models can only make use of observational data from existing battery management systems (BMSs). To facilitate model development, we release three large-scale datasets collected from the EV data platform hosted by Tsinghua University. Vehicles in each of our three released datasets are of the same make. We generate a random code name for each manufacturer and summarize the data statistics in Fig. 1a. Each charging snippet of a vehicle stores current, voltage and temperature as time series (Fig. 1b). Vehicle-level fault labels are generated from drivers' reports and confirmed by engineers based on the identification of lithium plating, low electric range, over-high temperature or unexpected voltage changes (too low, inconsistent among cells, etc.). These labels are created case-by-case and cannot be described by rule-based expressions on data.

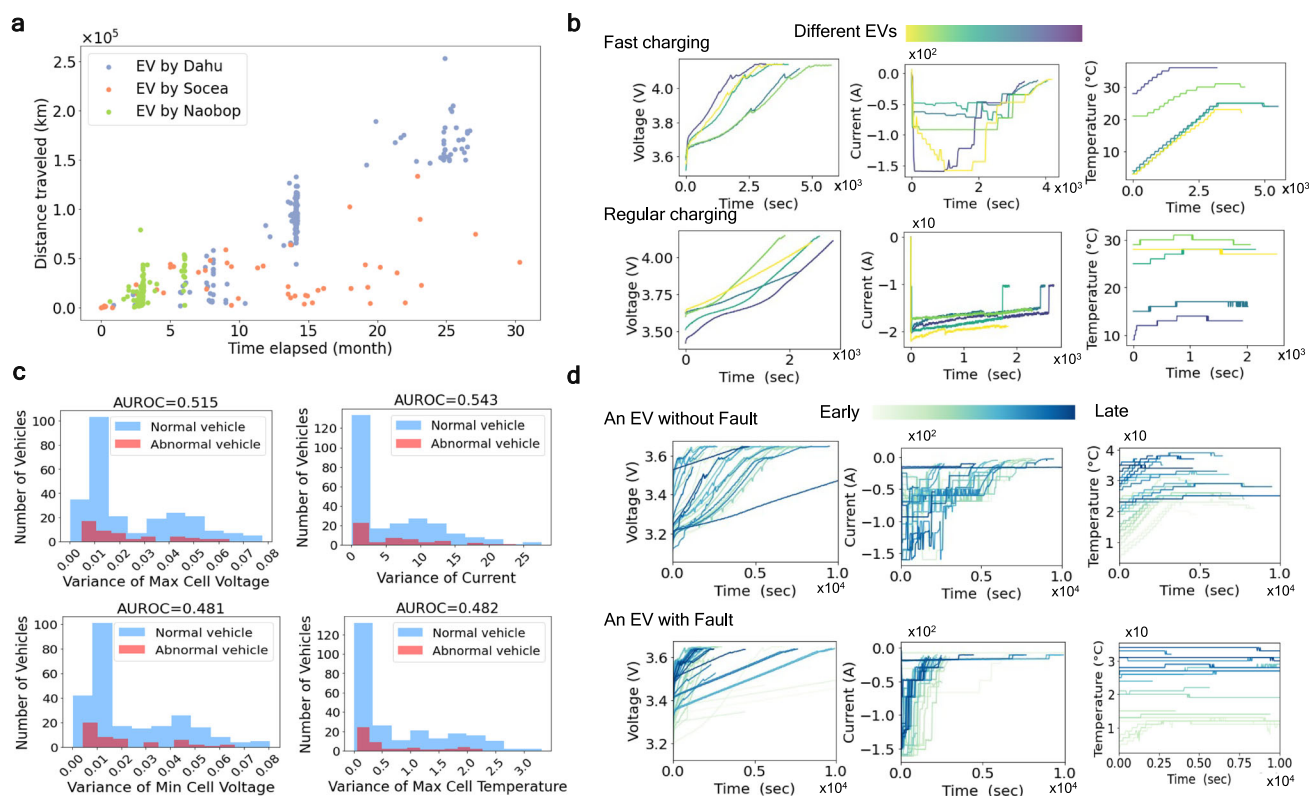
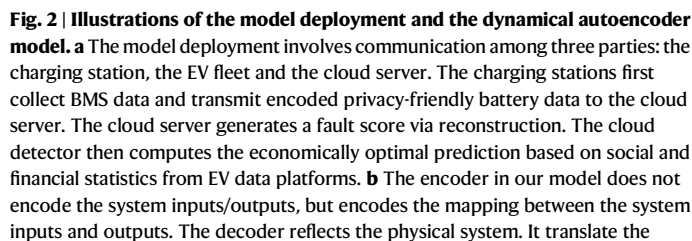


Fig. 1 | EV dataset and challenges in fault detection. **a** The data used in this study contains vehicles from three manufacturers, aliased Dahu, Socea and Naobop. Each dot represents the amount of data between the first charging record and the last charging record of a single vehicle. The x-value and y-value of a dot indicate the distance traveled and the time elapsed in records. **b** Sampled charging segments show that real-world charging patterns are diverse and irregular. Charging modes can be categorized into fast charging and regular

charging based on the level of the current. **c** Normal and abnormal EVs are poorly differentiated with canonical features such as the variance in cell voltage, current, or temperature, as an AUROC (area under receiver operating characteristic) around 0.5 can be achieved by random guesses. Higher AUROC value indicates greater prediction power. **d** A detailed view of LiB charging snippets from two sampled EVs. The comparison suggests that there is no simple feature to detect EV fault.



3

(specific charging state with a certain current). To address this issue, we propose the dynamical autoencoder for anomaly detection customized for anomaly detection on dynamical systems. Our model also adopts an encoder-decoder structure (see Fig. 2b) but the decoder, rather than constructing the entire data from the latent variables, now decodes the system response from the system input (see Supplementary Fig. 1 for an example). This intuition can be formalized by viewing the LiB data as collected from random nonlinear dynamical systems described by hidden Markov models (see Supplementary Note 1). Exploiting this structure customizes the general deep learning model for the LiB data. The dynamical autoencoder model is shown in Fig. 2c. The system control inputs include state of charge (SOC) and current, and system response include voltage and temperature. The encoder maps inputs (SOC, current) and outputs (voltage, temperature) into the latent variables that represent system parameters. Our model then detect system anomaly based on the discrepancy between the reconstructed and the observed system responses. In addition, auxiliary losses are added to achieve latent space regularization as in variational autoencoder and to provide weak supervision via mileage data (adding vehicle range as input).

A second problem for EV LiB data is that abnormal vehicle labels are sparse and made at the vehicle level; therefore, the labels may not truthfully reflect the condition of each data point corresponding to a particular charging snippet. To address this, we developed a robust scoring procedure (see Methods) to generate vehicle-level predictions from charging snippet predictions. The designed robust scoring procedure is parametrized by two hyperparameters τ and p , which predicts whether a charging snippet is abnormal by thresholding the reconstruction error at value τ and then predicts whether a vehicle is abnormal by averaging the top p percentile errors. The training pipeline is summarized in Fig. 2c.

Comparison against state-of-the-art algorithms

We compare our proposed algorithm against the widely used baselines including the graph deviation network (GDN), vanilla autoencoder (AE), support vector data description (SVDD), Gaussian process model (GP) and a data-driven battery fault detection algorithm (variation evaluation, VE) on the released datasets. The implementation details of the methods are provided in the Supplementary Note 2 and Supplementary Fig. 5. The detection performance, which is measured by the area under receiver operating curve (AUROC) based on the true positive rate and false positive rate, is provided in Fig. 3 and Table 1. The results show that the proposed dynamical autoencoder approach achieves the best detection results by a 16–33% AUROC boost (Fig. 3a) and a smaller variance compared to other algorithms (Table 1). The results also show that the auxiliary loss can further improve the detection performance (Fig. 3b). In addition, as depicted in Supplementary Fig. 2, the charging snippets from a normal vehicle and a faulty vehicle are rather difficult to be differentiated and are frequently falsely classified by the baselines. In contrast, the dynamical formulation in dynamical autoencoder can correctly pinpoint the charging snippets from both the normal and faulty vehicles.

The enhanced detection performance of the proposed dynamical autoencoder approach can lead to large economic advantages. We obtain the ranges of LiB fault rate based on the reported battery incidents provided to Tsinghua by EV manufacturers which we cannot disclose due to anonymization requests. The fault rate is estimated from 1.2 million EVs across major cities including Beijing, Shanghai, Guangzhou and Shenzhen. We further estimate fault cost, and inspection cost estimated from Circue's data obtained via partnership with insurance companies in China. Based on the average fault rate, the cost information and the ROC curves, we compute the expected direct costs of LiB fault and inspection (see Methods), as shown in Fig. 3c. The results show that optimally configuring the algorithm along the ROC curve has significant impacts on the overall costs. For all deep learning

algorithms (DyAD, GDN, AE, and SVDD), the expected direct costs first decrease and then increase. The best true positive rate of DyAD is ~50%. The minimum cost of the six algorithms (DyAD, GDN, AE, SVDD, GP and VE) is also provided by optimizing the true positive rate, as shown in Fig. 3d. In average, our DyAD reduces the expected direct costs by 33% when compared with the state-of-the-art deep learning algorithms, and 50% when compared with VE, a non-deep-learning method.

In high fault rate scenarios, the inspection scale would have an impact on the reputation of the EV manufacturer and in turn the sales revenues, which we do not yet have solid data to analyze. Such social and financial values (fault rate, fault cost, direct and indirect inspection costs etc.) vary by regions, and we are not trying to provide an accurate model configuration for every region or company here. Rather, we highlight the significance of such practical factors in algorithm configuration, as proposed in our deep learning framework (Fig. 2).

Knowledge learned by the dynamical autoencoder model

A more transparent interpretation of the model prediction can provide advice for EV maintenance or even guide the LiB manufacturing process. To this end, we interpret the internal mechanism of the dynamical autoencoder model by visualizing the distributions of embedded snippets at three different layers: the input layer, the latent layer between the encoder and the decoder, and the output layer computed as the difference between the prediction and the observation. To this end, we visualize how the neural network activation values for each data point (a charging snippet in a vehicle) change across different layers of the deep model. The activation values serve as a high level representation for each data, but is high-dimensional. Therefore, we use t-distributed stochastic neighbor embedding, a nonlinear dimension reduction technique, to project each charging snippet onto a 2D plane for each layer, as shown in Fig. 4.

More specifically, we choose an arbitrary vehicle and highlight the dimension-reduced representations of its LiB charging snippets in red and blue (indicating that the snippets are abnormal and normal, respectively), as in Fig. 4a–c. Snippets of other vehicles are colored gray. In Fig. 4c, the same red and blue points are plotted at the output layer, and other data points are further labeled based on whether they are normal (green) or not (purple). Data points that are closer together has similar semantic meaning to the neural network. We observed that while the snippets of different colors are jumbled in the input and latent layers (Fig. 4a, b), the deep model can successfully separate normal snippets from abnormal snippets in the output layer (Fig. 4c).

To illustrate the above observation with a more concrete example, three LiB charging snippets are picked and marked as \blacktriangle , \star , and \bullet . In Fig. 4d, we plot the predicted and observed curves of these three data points. In particular, two quantities, the LiB temperature and voltage, are presented to illustrate the errors between the predicted and observed curves. As shown in the right bottom figure of Fig. 4d, the two abnormal snippets (\blacktriangle , \star) have larger prediction errors. The embeddings of the data points are labeled in Fig. 4a–c. We note that the abnormal snippets are far apart in the input and latent layers, but become adjacent in the last output layer, which indicates that the designed prediction errors are good features for clustering abnormal snippets. Hence, based on the prediction errors, our DyAD model can determine an adaptive threshold intelligently, filter the abnormal snippets by ranking reconstruction errors, and accurately detect potential battery faults.

Discussion

In summary, the research work presented here aims to address the LiB fault detection problem by proposing a realistic deep learning pipeline and releasing a large-scale EV fault datasets with more than 690,000 charging snippets. Our model runs on existing BMS data, and can be readily deployed in real-world settings. Our model adopts dynamical

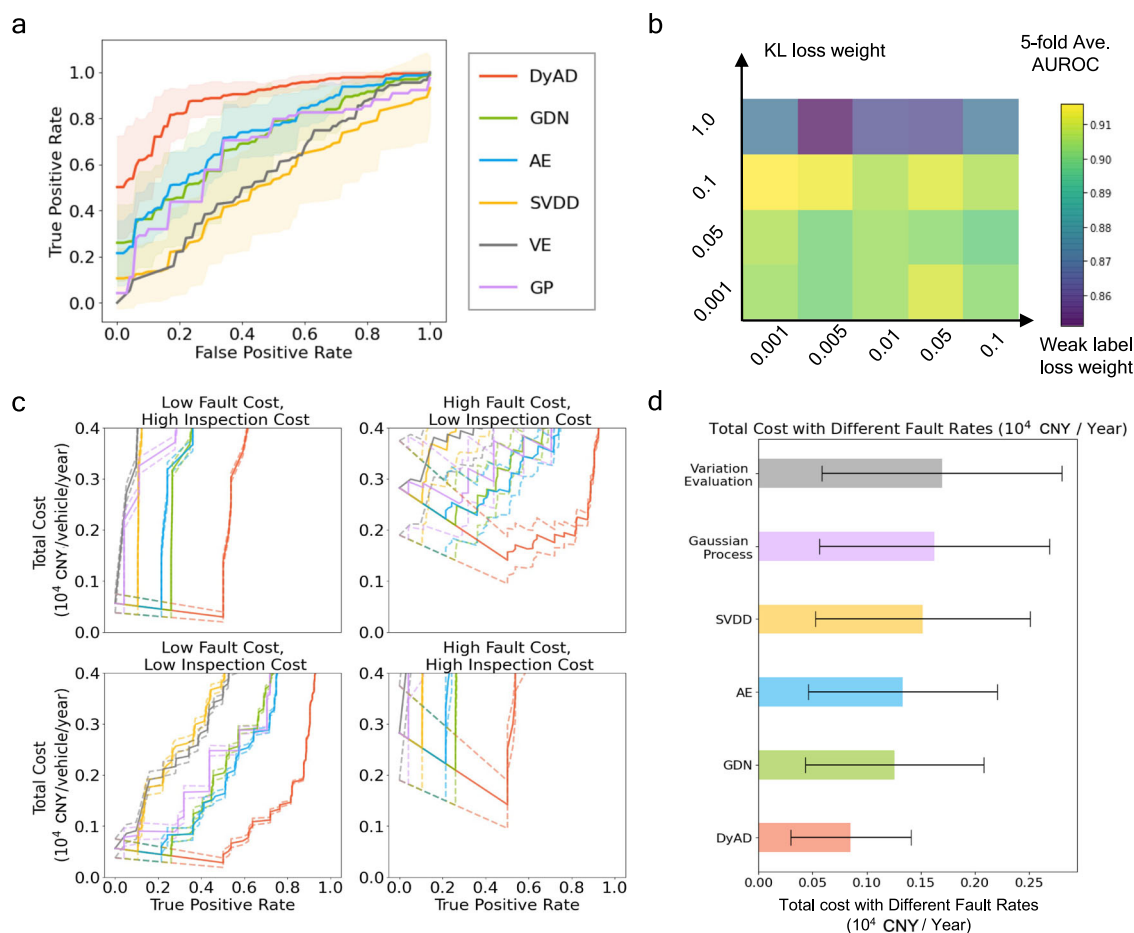


Fig. 3 | Evaluating prediction accuracy and EV battery cost. a The average ROC curves for the five algorithms. The solid curves indicate the average values out of five cross validation runs, and the shaded regions indicate the standard deviations of the trials. Our proposed procedure (orange) significantly outperforms other deep learning baselines (green, blue, yellow) and the standard variation evaluation method (gray). **b** The five-fold average AUROC of our proposed DyAD with different weights of the auxiliary training losses (KL regularization and mileage label loss). The variation of the average AUROC indicates that the auxiliary training losses

can nontrivially improve our model performance. The cost ranges can be found in Methods. **c** The sum of direct fault cost and inspection cost for EV batteries based on the statistics (battery fault rate, battery fault cost and vehicle inspection cost) we collected from an EV platform. The horizontal axis indicates the true positive rate achieved by each model for the corresponding cost value. **d** The minimum cost achieved for each algorithm by optimizing the total cost against the true positive rate. The confidence range is evaluated from our estimation of the vehicle fault rate (from 0.038% to 0.075%).

formulation and robust scoring, and can improve the detection performance upon existing procedures. It also reduces the expected direct fault and inspection costs by 33–50%.

We highlighted the role of social and financial statistics, specifically the fault rate and the direct costs of EV battery fault and inspection, in configuring our deep learning model. Such statistics may

vary by region, battery chemistry and manufacturer, thus the learning framework should be adaptive to the heterogeneity in these factors. While indirect costs may be hard to accurately capture, they are functions of the base fault rate, inspection scale, market share, etc. Each EV company might strategically project the indirect costs into their models and update them dynamically.

The data privacy of the EV owner and manufacturer is central to the large-scale application of EV fault detection. By deploying encoders and decoders separately at EV charging stations and the cloud, data are automatically encrypted and privacy-friendly. In addition to consumer data protection, this deployment structure also enables EV manufacturers to cooperatively train the encoder without direct data sharing and design a decoder that is adaptive to their own social and financial statistics.

We believe that our dataset and pipeline can serve as a first step for the artificial intelligence and the energy communities to jointly address the safety of EVs, especially given that many problems remain unsolved. One open ended and important problem is model interpretation. A more transparent interpretation in the language provided by battery mechanism research could provide advice for EV maintenance or even guide the battery manufacturing process. For example, besides SOC, current, voltage, and temperature used in this work,

Table 1 | Mean and standard variance of AUROC (%) values of considered algorithms

Algorithm	AUROC (%)	Average Direct Cost (10 ⁴ CNY)
DyAD	88.6 ± 2.9	0.085
GDN	70.3 ± 5.5	0.126
AE	72.8 ± 13.4	0.133
SVDD	51.5 ± 8.26	0.152
GP	66.6	0.162
VE	55.6	0.169

Our proposed method is highlighted in bold. The average direct costs of fault and inspection are in the unit of 10⁴ CNY/vehicle/year and calculated using the mean of the cost ranges. The VE and GP method has little internal randomness and hence no variance is reported.

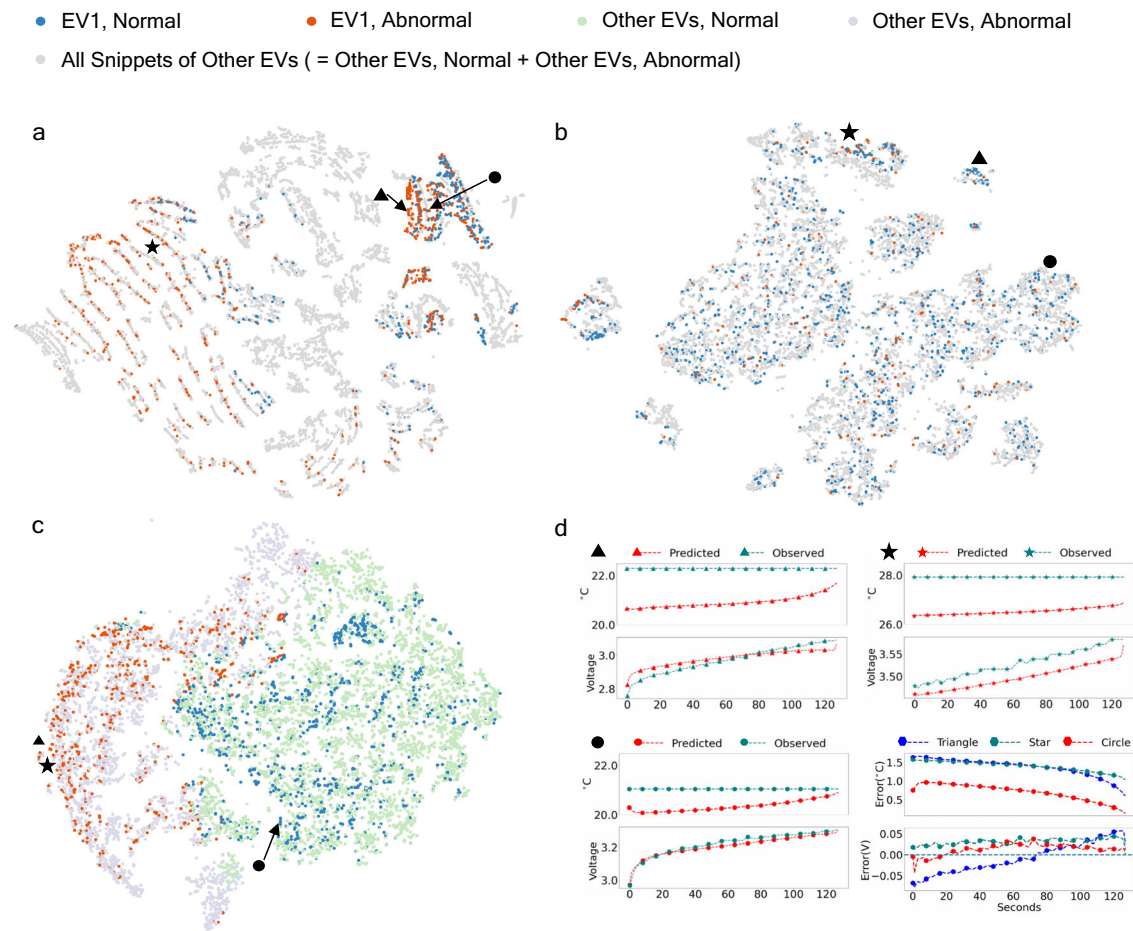


Fig. 4 | The evolution of embeddings of all fifteen abnormal vehicles in Dataset Dahu from the input layer to the output layer of the dynamical autoencoder model with t-distributed stochastic neighbor embedding visualization. Each subplot visualizes the dimension-reduced data of (a) the data input, (b) the inferred latent variable, and (c) the reconstructed observation. All snippets are identified as either abnormal or normal ones, marked as purple or green points in the output

layer, respectively. One EV (named EV1) is highlighted. Its snippets are marked as red and blue points according to their abnormality determined by the dynamical autoencoder model. The predicted and observed curves of the three snippets (marked as ▲, ★, and •) selected from EV1 include two dimensions: maximum battery temperature, and minimum cell voltage. **d** The predicted, observed, and corresponding error curves of three charging snippets marked as ▲, ★, and •.

the dynamics of more physics-informed battery parameters, such as capacity and internal resistance, could be estimated³⁴ or embedded in our model for battery safety with real-world data. Another challenging problem is to quantify the forecast horizon, as it would be beneficial to know for how long the model can predict battery problems in advance. We show in Supplementary Figs. 3 and 4 that the anomalies were detected through out the records, and hence it is difficult to determine the forecast horizon. Moreover, while this work has focused on the application of dynamical deep learning with robust scoring for EV LiB fault detection, such deep learning framework is promising for other fault detection tasks, particularly those for dynamical systems such as photovoltaic panels³⁵, robotic navigation³⁶, water treatment physical test-bed systems³⁷, and spacecraft³⁸.

Methods

Dynamical autoencoder

We provide more details on applying the dynamical autoencoder model to detecting battery anomalies. The dynamical autoencoder contains three groups of parameters: the parameters for the encoder θ , the parameters for the decoder ζ and the parameters for the multiperception head ξ . The encoder and the decoder are parameterized by GCN networks³⁹. All parameters are optimized with minibatch stochastic gradients to reduce a total training loss with three components: the reconstruction loss, the regularization loss and the mileage

supervision loss, as illustrated below,

$$l(\xi, \zeta, \theta) = l_{\text{recon.}}(\zeta, \theta) + l_{\text{reg.}}(\theta) + l_{\text{mileage}}(\xi, \theta). \quad (1)$$

More formally, the reconstruction loss for a single data snippet (x_0, x_1) is defined as

$$l_{\text{recon.}}(\theta, \zeta, x_0, x_1) = \text{MSE}(\text{Decoder}_{\theta}(\zeta, x_0), x_1), \text{ where } z = \text{Encoder}_{\zeta}(x_0, x_1). \quad (2)$$

In the above equation, x_0 denotes the input signal (i.e., the current and the SOC), x_1 denotes the system response (e.g., min voltage, max voltage, average voltage, min temperature and max temperature), z denotes the latent variable that represents the state of the dynamical system and MSE stands for the mean squared error.

In addition, as in the case for variational autoencoders⁴⁰, KL regularization is used to the latent space to avoid overfitting⁴¹,

$$l_{\text{reg.}}(\theta, x_0, x_1) = \|z_{\mu}\|^2 + \text{tr}(z_{\sigma}^2) - \log(|z_{\sigma}^2|), \text{ where } z = \text{Encoder}_{\zeta}(x_0, x_1) : z = [z_{\mu}, z_{\sigma}]. \quad (3)$$

Note that the latent variable is partitioned into $[z_{\mu}, z_{\sigma}]$ and represents the parameters of the distribution of the random dynamical system. We refer the reader to the supplementary material for a more detailed discussion.

Last, a mileage supervision is also added to guide learning.

$$l_{\text{mileage}}(\theta, z, x_0, x_1) = \text{MSE}(\text{MLP}_\xi(\text{Decoder}_\theta(z, x_0)), \text{mileage}), \quad (4)$$

where $z = \text{Encoder}_\zeta(x_0, x_1)$.

The impact of the mileage supervision is illustrated in Fig. 3b and it shows that asking the encoder to keep the mileage information can boost performance.

In our proposed deep learning pipeline, the encoder and decoder models adopt the GRU⁴² model with three layers and 32 hidden dimensions. The latent space between the encoder and decoder has 32 dimensions. The model is trained with the Adam⁴³ optimizer, in which the learning rate is set to be 0.001 and each minibatch contains 128 samples.

Robust scoring technique. In particular, we predict whether a charging snippet is abnormal by thresholding the reconstruction error at value τ and then predict whether a vehicle is abnormal by averaging the top p percentile errors. Both τ and p are finetuned on the training dataset. In particular,

$$L_{\text{vehicle}} = (l_1(\theta, \zeta, x_0, x_1), \dots, l_m(\theta, \zeta, x_0, x_1)), \text{ where } m = \text{number of snippets},$$

$$\text{Vehicle Error} = \left(\sum_{i=1}^n L_{\text{vehicle}}(i) \right) / n, \text{ where } n = p \times m.$$

A vehicle is abnormal, if $\text{Vehicle Error} > \tau$.

(5)

L_{vehicle} denotes all the reconstruction loss of snippets ranking in one vehicle, m denotes the amount of snippets of this vehicle, and Vehicle Error denotes the averaged reconstruction error in the top p percentile.

Expected direct cost calculation. The expected direct costs of EV battery fault and inspection are calculated as:

$$J(p, c_f, c_r, q_{\text{TP}}, q_{\text{FP}}) = p(1 - q_{\text{TP}})c_f + [pq_{\text{TP}} + (1 - p)q_{\text{FP}}]c_r \quad (6)$$

where, p is the fault rate of an EV battery; c_f is the direct cost of an EV battery fault; c_r is the direct cost of EV battery inspection; q_{TP} is the true positive rate of an EV battery fault detection algorithm; and q_{FP} is the false positive rate.

According to information from EV battery monitors/operators, the EV battery fault rate p ranges from 0.038% to 0.075%; the direct cost of an EV battery fault c_f ranges from 1 to 5 million CNY per vehicle; and the direct cost of an EV battery inspection c_r ranges from 8 to 55 thousand CNY per vehicle. We use the lower and upper bounds of the above ranges to calculate the expected direct costs in scenarios with high/low fault rates, fault costs, and inspection costs, respectively.

Data availability

The raw EV data are protected and are not available due to data privacy laws. The processed EV data are available with <https://doi.org/10.6084/m9.figshare.23659323> at the link https://figshare.com/articles/dataset/Realistic_fault_detection_of_Li-ion_battery_via_dynamical_deep_learning_approach/23659323.

Code availability

The code can be downloaded from https://github.com/962086838/Battery_fault_detection_NC_github. We also provide an additional backup for both the code and the data together at <https://disk.pku.edu.cn:443/link/37D733DF405D8D7998B8F57E4487515A>.

References

- Shaffer, B., Auffhammer, M. & Samaras, C. Make electric vehicles lighter to maximize climate and safety benefits. *Nature* **598**, 254–256 (2021).
- Castelvecchi, D. Electric cars: the battery challenge. *Nature* **596**, 336–339 (2021).
- Bednar, J. et al. Operationalizing the net-negative carbon economy. *Nature* **596**, 377–383 (2021).
- Schmuch, R., Wagner, R., Hörpel, G., Placke, T. & Winter, M. Performance and cost of materials for lithium-based rechargeable automotive batteries. *Nat. Energy* **3**, 267–278 (2018).
- Nykqvist, B. & Nilsson, M. Rapidly falling costs of battery packs for electric vehicles. *Nat. Clim. Change* **5**, 329–332 (2015).
- Harper, G. et al. Recycling lithium-ion batteries from electric vehicles. *Nature* **575**, 75–86 (2019).
- Finegan, D. P. et al. The application of data-driven methods and physics-based learning for improving battery safety. *Joule* **5**, 316–329 (2021).
- Palacin, M. R. & de Guibert, A. Why do batteries fail? *Science* **351**, 1253292 (2016).
- Deng, J., Bae, C., Marcicki, J., Masias, A. & Miller, T. Safety modelling and testing of lithium-ion batteries in electrified vehicles. *Nat. Energy* **3**, 261–266 (2018).
- Ebner, M., Marone, F., Stampanoni, M. & Wood, V. Visualization and quantification of electrochemical and mechanical degradation in lithium-ion batteries. *Science* **342**, 716–720 (2013).
- Zhang, Z. et al. Capturing the swelling of solid-electrolyte interphase in lithium metal batteries. *Science* **375**, 66–70 (2022).
- Xiang, Y. et al. Quantitatively analyzing the failure processes of rechargeable Li metal batteries. *Sci. Adv.* **7**, eabj3423 (2021).
- Wu, H., Zhuo, D., Kong, D. & Cui, Y. Improving battery safety by early detection of internal shorting with a bifunctional separator. *Nat. Commun.* **5**, 1–6 (2014).
- Zhou, X. & Huang, J. Impedance-based diagnosis of lithium ion batteries: Identification of physical parameters using multi-output relevance vector regression. *J. Energy Storage* **31**, 101629 (2020).
- Ye, Y. et al. Ultralight and fire-extinguishing current collectors for high-energy and high-safety lithium-ion batteries. *Nat. Energy* **5**, 786–793 (2020).
- Yang, X.-G., Liu, T. & Wang, C.-Y. Thermally modulated lithium iron phosphate batteries for mass-market electric vehicles. *Nat. Energy* **6**, 176–185 (2021).
- Ge, S. et al. A new approach to both high safety and high performance of lithium-ion batteries. *Sci. Adv.* **6**, eaay7633 (2020).
- Li, D., Zhang, Z., Liu, P., Wang, Z. & Zhang, L. Battery fault diagnosis for electric vehicles based on voltage abnormality by combining the long short-term memory neural network and the equivalent circuit model. *IEEE Trans. Power Electron.* **36**, 1303–1315 (2020).
- Hong, J., Wang, Z. & Yao, Y. Fault prognosis of battery system based on accurate voltage abnormality prognosis using long short-term memory neural networks. *Appl. Energy* **251**, 113381 (2019).
- Xue, Q. et al. Fault diagnosis and abnormality detection of lithium-ion battery packs based on statistical distribution. *J. Power Sources* **482**, 228964 (2021).
- Zheng, Y. et al. Micro-short-circuit cell fault identification method for lithium-ion battery packs based on mutual information. *IEEE Trans. Ind. Electron.* **68**, 4373–4381 (2020).
- Zhao, Y., Liu, P., Wang, Z., Zhang, L. & Hong, J. Fault and defect diagnosis of battery for electric vehicles based on big data analysis methods. *Appl. Energy* **207**, 354–362 (2017).
- Yang, R., Xiong, R., Ma, S. & Lin, X. Characterization of external short circuit faults in electric vehicle Li-ion battery packs and prediction using artificial neural networks. *Appl. Energy* **260**, 114253 (2020).
- Zhao, J., Ling, H., Wang, J., Burke, A. F. & Lian, Y. Data-driven prediction of battery failure for electric vehicles. *IScience* **25**, 104172 (2022).
- Couto, L. D., Reniers, J. M., Howey, D. A. & Kinnaert, M. Detection and isolation of small faults in lithium-ion batteries via the

- asymptotic local approach** Id couto would like to thank the wiener-anspach foundation for its financial support. this work was supported by the fond de la recherche scientifique-fnrs under grant no. 0142.20. In: *Proc. American Control Conference (ACC)*, 4434–4440 (IEEE, 2021).
26. Mnih, V. et al. Human-level control through deep reinforcement learning. *Nature* **518**, 529–533 (2015).
 27. He, K., Zhang, X., Ren, S. & Sun, J. Delving deep into rectifiers: surpassing human-level performance on imagenet classification. In: *Proc. IEEE International Conference on Computer Vision*, 1026–1034 (2015).
 28. Vaswani, A. et al. Attention is all you need. *Adv. Neural Inform. Process. Syst.* **30**, 5998–6008 (2017).
 29. Jumper, J. et al. Highly accurate protein structure prediction with alphafold. *Nature* **596**, 583–589 (2021).
 30. Ward, L. et al. Principles of the battery data genome. *Joule* (2022).
 31. Sulzer, V. et al. The challenge and opportunity of battery lifetime prediction from field data. *Joule* **5**, 1934–1955 (2021).
 32. Phan, N., Wang, Y., Wu, X. & Dou, D. Differential privacy preservation for deep auto-encoders: an application of human behavior prediction. In *Proc. Thirtieth AAAI Conference on Artificial Intelligence* (2016).
 33. Malekzadeh, M., Clegg, R. G., Cavallaro, A. & Haddadi, H. Mobile sensor data anonymization. In: *Proc. International Conference on Internet of Things Design and Implementation*, 49–58 (2019).
 34. Aitio, A. & Howey, D. A. Predicting battery end of life from solar off-grid system field data using machine learning. *Joule* **5**, 3204–3220 (2021).
 35. De Benedetti, M., Leonardi, F., Messina, F., Santoro, C. & Vasilakos, A. Anomaly detection and predictive maintenance for photovoltaic systems. *Neurocomputing* **310**, 59–68 (2018).
 36. Wellhausen, L., Ranftl, R. & Hutter, M. Safe robot navigation via multi-modal anomaly detection. *IEEE Robot. Autom. Lett.* **5**, 1326–1333 (2020).
 37. Deng, A. & Hooi, B. Graph neural network-based anomaly detection in multivariate time series. In: *Proc. Thirty-Fifth AAAI Conference on Artificial Intelligence*, 4027–4035 (AAAI Press, 2021). <https://ojs.aaai.org/index.php/AAAI/article/view/16523>.
 38. Hundman, K., Constantinou, V., Laporte, C., Colwell, I. & Söderström, T. Detecting spacecraft anomalies using lstms and nonparametric dynamic thresholding. In: Guo, Y. & Farooq, F. (eds.) *Proc. 24th International Conference on Knowledge Discovery & Data Mining*, 387–395 (ACM, 2018). <https://doi.org/10.1145/3219819.3219845>.
 39. Dauphin, Y. N., Fan, A., Auli, M. & Grangier, D. Language modeling with gated convolutional networks. In: *Proc. International Conference on Machine Learning*, 933–941 (PMLR, 2017).
 40. Kingma, D. P. & Welling, M. Auto-encoding variational bayes. *International Conference on Learning Representations* <https://iclr.cc/archive/2014/conference-proceedings/> (2014).
 41. Bergmann, P., Fauser, M., Sattlegger, D. & Steger, C. Mvtec ad—a comprehensive real-world dataset for unsupervised anomaly detection. In: *Proc. IEEE/CVF Conference on Computer Vision and Pattern Recognition*, 9592–9600 (2019).
 42. Cho, K. et al. Learning phrase representations using rnn encoder-decoder for statistical machine translation. In: *Proc. Conference on Empirical Methods in Natural Language Processing* (2014).
 43. Kingma, D. P. & Ba, J. Adam: a method for stochastic optimization. In *ICLR (Poster)* (2015).

Acknowledgements

This work was supported by National Key Research and Development Program of China under grant number 2022YFB2405600, the Tsinghua University Initiative Scientific Research Program, the National Natural Science Foundation of China under grant number 62103220, 52177217, 72271008, and 62273197, the Beijing Natural Science Foundation under grant number 3212031, the International Science & Technology Cooperation Program of China under grant number 2019YFE0100200, and the Tsinghua-Toyota Joint Research Fund. We also acknowledge support by the State Grid Corporation of China, State Grid Jiangsu Electric Power Co., LTD. and State Grid Wuxi Power Supply Company.

Author contributions

J.Z. and G.H. conceived the research. J.Z., Y.W., H.H., and S.H. developed the algorithms. J.Z., H.H., S.H., C.W., and Y.Z. conducted numerical experiments. J.Z., S.H., C.W., Y.Z., and D.G. performed data collection and management. G.H. formulated the economic model. B.J., Y.W., and X.H. interpreted the results. All authors edited and reviewed the manuscript. G.H. and M.O. supervised the work.

Competing interests

The authors declare no competing interests.

Additional information

Supplementary information The online version contains supplementary material available at <https://doi.org/10.1038/s41467-023-41226-5>.

Correspondence and requests for materials should be addressed to Guannan He or Minggao Ouyang.

Peer review information *Nature Communications* thanks the anonymous reviewer(s) for their contribution to the peer review of this work. A peer review file is available.

Reprints and permissions information is available at <http://www.nature.com/reprints>

Publisher's note Springer Nature remains neutral with regard to jurisdictional claims in published maps and institutional affiliations.

Open Access This article is licensed under a Creative Commons Attribution 4.0 International License, which permits use, sharing, adaptation, distribution and reproduction in any medium or format, as long as you give appropriate credit to the original author(s) and the source, provide a link to the Creative Commons license, and indicate if changes were made. The images or other third party material in this article are included in the article's Creative Commons license, unless indicated otherwise in a credit line to the material. If material is not included in the article's Creative Commons license and your intended use is not permitted by statutory regulation or exceeds the permitted use, you will need to obtain permission directly from the copyright holder. To view a copy of this license, visit <http://creativecommons.org/licenses/by/4.0/>.

© The Author(s) 2023